1-24-2020

Scaling of Incidence Variations With Inlet Distortion for a Transonic Axial Compressor

D. J. Hill
University of Windsor

J. J. Defoe
University of Windsor

Scaling of Incidence Variations with Inlet Distortion for a Transonic Axial Compressor

D. J. Hill*

J. J. Defoe

Turbomachinery and Unsteady Flows Research Group

Department of Mechanical, Automotive, and Materials Engineering

University of Windsor

Windsor, ON N9B 3P4, Canada

e-mail: hill11g@uwindsor.ca

ABSTRACT

This paper numerically explores the manner in which blade row inlet incidence variation scales with a variety of distortion patterns and intensities. The objectives are to (1) identify the most appropriate parameter whose circumferential variation can be used to assess scaling relationships of a transonic compressor, and (2) use this parameter to evaluate two types of non-uniform inflow patterns, vertically stratified total pressure distortions and radially stratified total enthalpy and total pressure distortions. A body force model of the blade rows is employed to reduce computational cost; the approach has been shown to capture distortion transfer and to be able to predict upstream flow redistribution with inlet distortion. Diffusion factor is shown to be an inadequate proxy for streamline loss generation in non-uniform flow, leading to the choice of incidence angle variations as the metric for which we assess scaling relationships. Posteriori scaling of circumferential flow angle variation based on the maximum incidence excursion for varying distortion intensity yields an accurate method for prediction of the impact for other distortion intensities; linear regression of the maximum variation in incidence around the annulus as a function of distortion intensity had $R^2 > 0.97$ *for all spanwise locations examined in both the rotor and stator for both vertically and radially stratified distortions. However, changes to far upstream distortion shape yield highly non-linear incidence variation scaling; the results suggest that the pitchwise gradients of far upstream total pressure govern the degree of linearity for incidence variation scaling.*

1 Introduction

Fans and first stage compressors in modern and future aircraft may have a design point in which the rotor is subjected to continuous inlet flow distortion. Examples include boundary layer ingesting (BLI) fans and turboprop engines with different axes of rotation for the propeller and compressor. The typical impact of such distortions on single stage compressor isentropic efficiency is 1-2% [1]. Recent work [2] considered a parametric study of distortion impacts on low-speed fan performance but the computational approach was inviscid so efficiency changes could not be quantified. Instead, the authors used diffusion factor as a proxy for efficiency changes. In this paper we first identify the shortcomings of using diffusion factor as a proxy for loss for a transonic axial compressor in non-uniform flow. Following this, results of a parametric study similar to that carried out by Defoe et al. [2] are presented, but the performance metric of interest is variation in blade row inlet flow angles. The following brief review of pertinent literature identifies the knowledge gap this paper fills.

Fidalgo et al. [3] studied NASA stage 67, a transonic single-stage compressor, subjected to a 120° total pressure deficit. The work encompassed experimental and computational approaches, the latter using a full-annulus unsteady Reynolds-Averaged Navier-Stokes (RANS) simulation. The key finding was that the upstream influence of the rotor blade row, due to circumferentially non-uniform rotor work, allows the machine to operate at distortion intensities which would otherwise lead to stall due to locally high incidence. This non-uniform rotor work yields greater streamtube contraction for regions of lower incident total pressure, reducing the corresponding static pressure and subsequently introducing regions of co-swirl and counter-swirl as the flow redistributes around the spinner nose upstream of the rotor.

Gunn and Hall [1] investigated a total pressure distortion representative of BLI. As with Fidalgo et al. [3], the primary mechanism leading to flow redistribution was the non-uniform rotor work profile which assists in attenuating the upstream distortion intensity. Additionally, the authors were able to demonstrate that key distortion flow characteristics are shared by both low-speed and transonic fans so that qualitatively, the response of low-speed and high-speed machines is expected to be similar.

Hall et al. [4] employed a non-axisymmetric throughflow model in computational fluid dynamics (CFD) simulations to observe the performance of various fan stage design parameters in the presence of BLI-style distortion. Two key outcomes from this work were the verification of the low-fidelity computational model against both higher-fidelity calculations and experimental results from [1], as well as the finding that non-axisymmetric stator geometry provides the most promising solution for mitigating BLI performance loss. This finding was later confirmed by Gunn and Hall [5] by demonstrating a reduction in loss of 10% compared to clean, undistorted inflow by employing a non-axisymmetric stator design for a fan subject to BLI-type distortion.

As alluded to earlier, Defoe et al. [2] used an inviscid throughflow model to complete a parametric study of distortion patterns and intensities and assess the resultant effects for performance of a low-speed fan. The inviscid model required the authors to quantify performance changes in each blade row in terms of diffusion factor. The mechanism driving non-uniform rotor work in distortions of only total temperature was shown to be changes in local density, but large variations in total temperature on the order of 10% of the maximum value were required to produce significant effects. Additionally, in distortions with neither sharp pitchwise gradients in diffusion response nor strong radial flows, the response of the fan blade

rows to distortions of various intensities were shown to be predicted through linearly scaling up a low intensity distortion. Finally, the response for distortions of several inlet quantities were shown to be able to predicted based on summing the responses for the constituent distortions.

This paper builds upon the findings outlined above by considering a high-speed compressor for a similar parametric study of inlet distortions. To accomplish this, a body force-based numerical model of the compressor of interest is used based on the work of Hill and Defoe [6]. This approach is selected as it enables a reduction of computational cost of 2-3 orders of magnitude in comparison to full-annulus unsteady RANS computations. This cost reduction comes from both reduced grid size and, most importantly, from enabling a steady solution since the individual rotor blades' unsteadiness is no longer resolved. The authors adapted previous throughflow models using a calibrated compressibility correction factor to allow for use with a transonic compressor. For NASA stage 67, the model was shown to accurately predict rotor work input and isentropic efficiency in uniform flows. As well, for non-uniform flow, the model captures distortion transfer through the machine and the associated stage efficiency penalty.

The body force model is separated into two components: a normal turning force and a viscous loss force. The viscous loss force depends on the blade row inlet mass-averaged relative Mach number, as in Peters et al.'s viscous model [7],

$$f_p = \frac{K_{p1}}{b}\left[\left(\overline{M}_{rel}^{M}\right)^2 + K_{p2}\left(\overline{M}_{rel}^{M} - M_{ref}\right)^2\right] W^2, \tag{1}$$

where $\overline{M}_{rel}^{M}$ is the mass-averaged relative Mach number calculated on a plane of constant axial coordinate at the leading edge of the blade row, W is the velocity magnitude in a frame of reference moving with the blades, b is the staggered blade spacing, and the coefficients K_{p1}, K_{p2}, and M_{ref} are used to set the peak efficiency and the slope of the efficiency curve. The local loss force is dependent on the squares of the inlet relative Mach number and local relative velocity. In Hill and Defoe [6], two sets of coefficients are used to enable different rates of efficiency decrease on either side of peak efficiency. A limitation of this model was observed in non-uniform flows: it is unable to capture local deviations from the design flow coefficient. When the mass-averaged flow coefficient remains unchanged ($\overline{M}_{rel}^{M} \approx$ constant), but due to inlet distortion the local axial velocity varies, the model is unable to capture the local physical "loss bucket" behavior that is expected in a turbomachine. For this reason, local tracking of entropy generation along individual streamlines is not expected to be accurate and is avoided in the present paper.

In Defoe et al. [2], diffusion factor changes were used as a proxy for loss variations. Empirical observations from low-speed linear and annular cascades have demonstrated that, on-design, there exists a one-to-one relationship between diffusion factor and loss for a variety of blade designs as expressed via a loss parameter which combines loss coefficient, solidity, and flow angle information [8].

The objective of the work presented in this paper is to: (1) investigate the relationship between diffusion and loss off design, and (2) determine what scaling of distortion response can be observed for a transonic compressor.

The key findings of this paper are that (1) loss parameter is intended to be a on-design metric such that its relationship with diffusion factor breaks down for non-uniform inflow – as a result the scaling metric used in this work is blade row inlet flow angle variations, (2) changes to the shape of the far upstream distortion yield highly non-linear inlet flow angle variation scaling, especially for vertically stratified distortions, and (3) the inlet flow angle variations scale linearly with distortion intensity, especially when using a posteriori method of scaling the maximum flow angle excursions. Linear regressions yield R^2 values greater than 0.97 in all cases considered. Not only are the maximum excursions predicted but the flow angle variation around the annulus is also well-predicted using this approach, within the range of intensities considered.

The paper is organized in the following manner. Firstly, the machine of interest is presented. Following this, the relationship between diffusion and loss parameter is investigated for both uniform and non-uniform inflow and the scaling metric used in this work is discussed. Next, the computational approach used in the parametric study and the distortions of interest themselves are detailed. Finally, rotor and stator inlet flow angle variation scaling is investigated across the parametric range of distortions.

2 Machine of Interest

The computations in this work are carried out on a transonic axial compressor, NASA stage 67 [9]. The duct extends approximately one and a half rotor inlet diameters upstream of the rotor and downstream of the stator. A meridional view of the computational domain and axial measurement locations referenced throughout this paper is shown in Fig. 1. The computations are carried out at 90% of the design rotational speed, yielding a blade tip relative Mach number of 1.20 at the peak efficiency flow coefficient. The flow coefficient is based on inlet velocity and midspan blade speed,

$$\phi = \frac{\dot{m}}{\bar{\rho}_0^M A_0 U_{\text{mid}}}, \tag{2}$$

where $\dot{m}$ is the mass flow rate, $\bar{\rho}_0^M$ is the mass-averaged density, A_0 is the duct area at domain inlet, and U_{mid} is the midspan blade speed. Only a portion of the hub near the rotor rotates; the spinner nose is stationary. With a mean hub-to-tip radius ratio of 0.427, the stage is subject to significant radial flow streamline shifts, as expected in a first-stage compressor blade row. Rotor performance characteristics for this machine are given in Table 1 and geometric characteristics for both the rotor and stator can be found in Table 2.

3 Metric for Off-Design Behavior

To assess the performance of an axial turbomachine subjected to non-uniform inflow distortion, the increase in local streamline entropy generation from a uniform inflow baseline provides a strong indication of the distortion's impact on loss. As discussed in Sec. 1, this is not possible in this paper due to limitations specific to the viscous loss model employed. Additionally, the body force method employed is unable to accurately capture some characteristics of flow in an actual blade

row: tip leakage flows, shock losses, and downstream wake mixing. At the maximum efficiency operating point, the body force model can adequately capture these effects, but does less well as the operating point moves further off-design. For non-uniform inflow conditions, the local flow coefficient moves, in different regions, below and above the design operating condition if the mass-averaged flow coefficient is held constant at the design value. While the viscous loss model used in this work was shown to capture overall efficiency trends in non-uniform inflow [6], it inadequately captures local streamwise entropy generation. For this reason, an alternative method for quantifying distortion effects is required in this work.

Previous inviscid studies of fan response in inflow distortion such as in Refs. [2] and [4] have made use of diffusion factor as a means of predicting regions of increased blade loading. The diffusion factor is an idealization of the difference between the maximum velocity on the suction surface and the uniform trailing edge velocity. High diffusion factor corresponds to increased adverse pressure gradients and subsequent boundary layer growth, a rise in momentum thickness, and entropy generation [10]. Thus, increases in diffusion factor have been used as a proxy for increases in loss coefficient. In this paper the diffusion factor is defined as

$$D = 1 - \frac{W_{\text{out}}}{W_{\text{in}}} + \frac{r_{\text{out}} W_{\theta\text{out}} - r_{\text{in}} W_{\theta\text{in}}}{W_{\text{in}}} \frac{2\pi/B}{\overline{c}_{\text{in-out}}}, \tag{3}$$

where r is the streamtube radius and $\overline{c}_{\text{in-out}}$ is the local blade axial chord. The blade row axial chord is known as a function of radius at the leading and trailing edge. From this the local axial chord is estimated as

$$\overline{c}_{\text{in-out}} \approx 0.5 \left(c_{r_{\text{in}}} + c_{r_{\text{out}}} \right), \tag{4}$$

where $c_{r_{\text{in}}}$ and $c_{r_{\text{out}}}$ are the axial chord based on the radius of a streamline at the blade row leading and trailing edges, respectively.

Kerrebrock [8] describes the argument for a generalized correlation between loss parameter, Z, and diffusion factor. By assuming zero velocity in the discrete blade wakes and constant total pressure outside the wakes, the parameter which is expected to be a function only of diffusion factor can be shown to be

$$Z = \zeta_i \frac{cos\beta_{i+1}}{2\sigma} \left(\frac{cos\beta_{i+1}}{cos\beta_i} \right)^2, \tag{5}$$

where ζ_i is the loss coefficient based on inlet conditions, β_i and β_{i+1} are the inlet and outlet relative flow angles, respectively,

and σ is the solidity. Experiments on low-speed annular cascades have shown that indeed Z is approximately a unique function of D [11]. The correlation was shown to hold at design conditions for uniform inflow, using mass-averaged quantities for the whole cascade at blade row inlet and exit. For a stator the flow angles are those in the stationary frame. In this paper we use the the entropy-based loss coefficient for ζ_i, which for a rotor between stations i and $i+1$ is defined as

$$\zeta_i = \frac{T_{ti}^{rel} \Delta s_{(i+1)-i}}{\left(h_{ti}^{rel} - h_i\right)}, \tag{6}$$

where T_{ti}^{rel} is the inlet relative total temperature, $\Delta s_{(i+1)-i}$ is the entropy rise across the blade row, and $(h_{ti}^{rel} - h_i)$ is the relative kinetic energy per unit mass at the blade row inlet. For a stator all quantities are taken in the stationary frame. We define this loss coefficient for each streamline through a blade row. To assess the validity of the assumption that $Z = f(D)$ in compressible, transonic flow, Z is plotted against D for stage 67 in Fig. 2 using a single-passage RANS computation at the peak efficiency flow coefficient of $\phi = 0.498$ at 90% of the design rotational speed. The single passage (SP) computations are carried out using ANSYS CFX 17.0 [12] on a grid created using Pointwise [13] for the upstream and downstream extents and TurboGrid [14] for the rotor and stator regions. This steady state computation utilizes the shear-stress-transport (SST) turbulence model [15] and a maximum y^+ value of 40. At the domain inlet, total conditions are specified and the flow direction is axial (the x direction). The static pressure is set at the domain outlet to achieve the desired operating condition. Two mixing planes are used: two rotor axial chords upstream of the rotor (to minimize interaction with the rotor blade leading edge) as well as between the rotor and stator blades, slightly downstream of the measurement plane 2. Initial grid sizing was based on previous work by Fidalgo et al. [3] on the same machine, to reduce the necessary grid refinement iterations. The initial grid was a 50% cell count increase compared to Fidalgo et al.'s and then the next sizing was another 38% increase in cell count. The convergence criteria considered were the rotor total pressure ratio and isentropic efficiency. Table 3 shows the change in these criteria between successive grids, where it is seen that the medium grid provides sufficiently grid independent results. The grid selected is 3.6 million cells including the upstream, rotor, stator, and downstream regions for a single rotor and stator passage.

The data in Fig. 2 is circumferentially averaged over a single pitch, but can be seen to vary significantly across the span. The span fraction increases in general with D and Z in the rotor; the opposite is true in the stator. The data is separated into three regions: inner span ($< 25\%$), mid span ($25\% - 75\%$), and outer span ($> 75\%$), based on measurement plane 1 streamline radius. For both the rotor and stator blade rows, the data is shown to nearly collapse to the empirical relationship between loss parameter and diffusion factor in the mid span region. For the rotor blade row, the associated diffusion factor range is smaller due to the design of the blade; mid span blade twist was tailored to produce near-uniform blade loading. In the stator, this mid span includes a wider range of diffusion but still agrees well with the empirical relationship. For both blade rows, the data begins to skew towards higher than expected loss parameter in the inner and outer spans. This can be attributed to several factors: endwall boundary layer losses, increased endwall radial streamline shifts, secondary flows on

the rotor hub and stator hub and casing, and rotor tip-leakage losses. The loss parameter is unable to capture the impact of these local flow features. In Fig. 3 a contour plot of the circumferentially averaged entropy function elucidates the effects above as it pertains to NASA stage 67. In this figure, it can be seen that the rotor tip leakage yields a significant local increase in entropy in the outer $3\% - 6\%$ span of the rotor. This then interacts with the casing endwall losses to create a region of increased loss spanning as much as the outer 13% of each respective blade row. The mixing plane location indicated is just downstream of the axial measurement plane used for the rotor outlet in this work. The data shown here illustrates why the loss parameter in Fig. 2 dramatically increases from the experimental trend in the outer 15% span (each data point corresponds to 1/60 span). Due to numerical stability issues, the hub wall in the rotor is set to zero shear stress, as explained in Hill and Defoe's prior work [6]. The effect of this is that the endwall influence region only begins to noticeably develop downstream of the mixing plane and is the reason why the lower 25% rotor span in Fig. 2 does not experience the stark increase in loss seen in the stator. However, in the inner 10% span in the rotor, there is a slight increase in entropy, arising from the hub boundary layer incident to the rotor upstream of the free-slip region. This region of increased entropy is convected through the rotor until it reaches the stator and endwall boundary layer effects once again generate loss.

Of importance to note from the above discussion is that the relationship between loss parameter and diffusion factor in the 25%-75% span region holds true for a transonic axial compressor, despite the derivation of Z from incompressible cascade flow assumptions. This is due to an adaptation of the diffusion factor (Eq. 3) by including radial shifts from inlet to outlet; the pressure variation on a streamtube across a blade row is dependent on the angular momentum, not just the angular velocity [8]. Therefore it is possible to make use of diffusion factor as a proxy for loss within the aforementioned span region for uniform inflow even for high-speed compressors. However, for the non-uniform inflows considered in this paper, nearly every location in both the rotor and stator is operating locally off design. To observe the effect of this on the relationship between diffusion factor and loss parameter, loss parameter from bladed single passage RANS computations are plotted at midspan for three different flow coefficients ($\phi = 0.472, 0.498$, and 0.520) against diffusion factor in Fig. 4. The shortcoming of using diffusion factor in this scenario can be seen in both blade rows. Increasing the flow coefficient reduces the local blade loading or diffusion factor, however it does not yield an associated decrease in loss parameter. Therefore changes in diffusion factor for non-uniform inflow are not expected to monotonically correspond to changes in loss parameter for compressors operating off-design. This is because diffusion factor is intended to be a design point metric [8].

The results in this section suggest that for the computational approach adopted in this paper, neither tracking local entropy generation nor using diffusion factor as a proxy for loss are feasible approaches for making inferences about performance in non-uniform flow for a transonic compressor. Rather, to assess machine performance in non-uniform flow, variations in inlet relative flow angles are utilized. A blade row is generally designed such that the efficiency is optimized for a particular incidence. As the local flow coefficient is pushed away from this design point, the response is generally a local increase in loss coefficient. Therefore, in non-uniform flow, local deviations from the circumferentially averaged relative flow angle suggest increases in loss coefficient, with a larger impact being observed for increased flow angle (incidence) due to the additional turning required. The body force model in this work has been demonstrated to accurately capture flow redistribution and blade row outlet flow angles, as shown in Figs. 5-7. A 120° sector of reduced total pressure was

compared against higher-fidelity unsteady (U)RANS performed by Fidalgo et al. [3]. Downstream of the rotor, the trends of both total temperature and flow angle are well predicted by the body force approach at midspan as can be seen in Fig. 5. The good agreement of the work input implies that the rotor inlet flow redistribution (variations in axial velocity and flow angle) is well-captured. This observation is supported by the work done by Hall et al. [4] who carried out analysis using a similar normal force modeling approach as that employed in this paper. In their work, they tested BLI type distortions both experimentally and computationally on the Whittle Laboratory Fan, a purpose built fan rig for observing the effects of BLI [1,16,17]. Immediately upstream of the rotor, they were able to demonstrate that the axial velocity is predicted to within 8% error and the absolute swirl angle is predicted everywhere within $< 1^{\circ}$. Returning to stage 67, in Fig. 6, which shows spanwise distributions of total temperature ratio and flow angle variations for a circumferential location in the middle of the distortion upstream of the rotor, the absence of a tip gap in the body force model is clear as it is unable to predict the outer span flow angles and as a result, the flow angles are generally overpredicted in the majority of the blade span to compensate for this; the overall blade row work input is matched. However, the trend of flow angle from 20% to 80% span is consistent with the URANS results. In Fig. 7, the observations made above are seen to hold true for the stator as well, as the body force model does an excellent job predicting outlet flow angles aside from individual blade wakes.

Since the variations in inlet flow angle are well-predicted by the body force model and the effect of incidence variation on an axial compressor's loss coefficient is well known to result in a "bucket-like" behavior, we proceed to study distortion impact using variations in blade row inflow direction.

4 Approach for Parametric Study of Inflow Distortions

This section outlines the approach used in the parametric study of two distinct distortion types. The computational methodology used to complete this study is discussed and following this the selected distortion matrix is presented.

4.1 Computational Approach for Non-Uniform Flows

The computational cost associated with full annulus computations of non-uniform inflow is significantly reduced by making use of a body force model. The model employed in this work is that developed by Hill and Defoe [6]. Body force models replace physical blade rows with a swept volume of body forces representative of the blade work input and viscous losses. The result is a pitchwise smeared-out average of flow in each blade passage. Full details of the model and its implementation can be found in Ref. [6]. Eliminating the physical blades allows for a reduction in grid density of approximately two orders of magnitude. More significantly, distortion transfer can be captured in a steady computation. These computational cost reductions render tractable the many computations carried out for this work. In non-uniform inflow, the specific model employed was shown in Ref. [6] not only to capture distortion transfer (see Figs. 5 and 7) but also overall efficiency penalties associated with inlet flow distortion. For distortion transfer to be well captured with this approach, the flow non-uniformity must have a characteristic length scale significantly larger than a single blade pitch and the local rotor reduced frequency must be significantly less than one [4]. That is,

$$g_{red} = \frac{c_x/V_x}{2\pi/\Omega} \ll 1, \tag{7}$$

where c_x is the axial chord, V_x is the axial velocity, and Ω is the rotational speed. This implies that the time it takes for the flow to travel through a blade passage must be significantly less than the time for one rotor revolution. The maximum value for NASA rotor 67 is 0.06 for the inflows considered in this paper.

Pointwise [13] is used for grid generation and all computations are carried out with ANSYS CFX 17.1 [12] as the solver. Source terms are implemented in the rotor and stator swept volumes as momentum and (for the rotor) energy sources. The shear stress transport (SST) turbulence model is used and a y^+ roughly set to 40 is used along the end-wall regions. As detailed by Hill and Defoe [6], adverse pressure gradients coincide with discontinuous changes in hub radius curvature in the rotor of NASA 67. For this reason, slip wall conditions are used in the same way as in the single passage computation discussed earlier to avoid nonphysical flow separation. This is not of significant consequence in this study as the body force viscous loss model accounts for end-wall losses within the blade rows; hub and casing boundary layer flow features are not of primary interest. At the inlet, total pressure, total temperature, and axial flow are specified; static pressure is set at the domain outlet to achieve the desired flow coefficient.

A grid independence study was conducted over a series of five grids. The results of rotor work input at peak efficiency are presented in Fig. 8 as circles on the left axis, plotted against the inverse of cell count, N. As grid cell count moves towards infinity, this quantity should approach its theoretical grid independent value. It is shown that this rotor work input achieves a state of grid independence at only the second level of grid density; further refinements (moving left on the plot) yield negligible changes in work input. For this reason, the second level of grid density is used for the work in this paper. Due to the nature of the viscous loss model employed, there is no grid independent efficiency value. Entropy generation in the body force regions is highly dependent on the grid discretization itself for a given set of model coefficients. Instead, the loss model coefficients are tuned to achieve the correct loss for the selected grid. This effect is observed through the rotor isentropic efficiency plotted as crosses on the right axis of Fig. 8. Each of these data points are generated using the tuned loss coefficients of the selected grid. The sensitivity of the loss model to grid discretization reveals itself as a maximum mismatch in efficiency of $\sim 2\%$ is observed. The full annulus grid consists of 4.48×10^6 cells, a reduction of over 90% compared to the bladed URANS computational domain used by Fidalgo et al. [3] on the same machine.

4.2 Inlet Distortions Considered

Qualitatively similar distortions to those in the work of Defoe et al. [2] are considered in this paper. The intensities of the distortions are scaled up to account for the significant increase in blade speed (low-speed fan versus transonic compressor). These distortions are of two types, vertically stratified and radially stratified.

The vertically stratified distortions emulate BLI aircraft configurations where low momentum airflow over the airframe

is ingested by aft-placed engines. The distortions are characterized by two parameters: (1) the intensity of the distortion, $p_{t,\max}/p_{t,\min}$, and (2) the immersion of the distortion across the duct inlet diameter, $\delta/2R_0$. A schematic of this type of distortion is shown in Fig. 9, which also gives the convention for circumferential angle θ and shows the direction of rotor rotation. The ratio of maximum to minimum total pressure in the distortion is the appropriate metric for quantifying intensity in compressible flow, in a similar manner that a metric based on the difference in total pressure was used for incompressible flow in Defoe et al. [2].

The radially stratified distortions are idealized representations of the flow non-uniformity a first compressor stage might experience in a turboprop engine, where the propeller axis is offset from the compressor axis. The hypothetical propeller produces a radially non-uniform work distribution which is then passed on to the first stage compressor. The associated inlet swirl is neglected in this paper. The two parameters which define these distortions are (1) the spacing between the propeller axis and compressor axis, ΔR, as well as the magnitude of the radial work input gradient. A schematic of the radially stratified distortions is illustrated in Fig. 10, where r' is the radial coordinate measured from the center of the distortion. At the hypothetical propeller tip, $r'/R_0 = 8$, the total pressure and total enthalpy are related isentropically, and from those values both p_t and h_t are scaled down linearly to a minimum value at the propeller hub.

The specific distortions studied are listed in Table 4. Small differences in total pressure distortion intensity are observed for the combined distortions of varying offset values. This arises from changes in mass averaged density due to the total enthalpy distortion; flow coefficient is the quantity held constant.

5 Results of Parametric Study of Inflow Distortions

Flow redistribution mechanisms are found to be the same between low-speed and transonic compressors, consistent with Gunn and Hall's findings [1]. Therefore the manner in which each distortion interacts with the turbomachinery is not discussed in detail here; the interested reader is referred to Ref. [1] for an in-depth analysis for vertically stratified distortions and to Defoe et al. [2] for radially stratified distortions. Since it is possible to design blades for any average inflow angle, in this section, variations from circumferential means are considered rather than comparisons against uniform inflow. The local change in relative flow angle in the rotor is

$$\Delta\beta = \beta - \overline{\beta}^{\theta}, \tag{8}$$

where $\overline{\beta}^{\theta}$ is the circumferentially-averaged relative flow angle at a given inlet span fraction. For the stator, this parameter is expressed in the stationary frame as $\Delta\alpha$. To track quantities along streamlines in non-uniform flow, a series of uniformly spaced streamlines are seeded at the computational domain inlet and tracked as illustrated in Fig. 11. The non-uniform streamline radial shifts can clearly be seen. The seeding pattern consists of 120 circumferential and 60 spanwise seeds at the domain inlet, rotor inlet, and stator inlet. Data is then extracted along each of the streamlines at the relevant downstream

axial locations and quantities are plotted based on the upstream seed location.

5.1 Vertically Stratified Distortion: Intensity Variation

The intensities considered are $p_{t,\max}/p_{t,\min} = 1.050, 1.093,$ and 1.122 as indicated in Table 4. In Fig. 12 the resulting incidence variations for $\delta/2R_0 = 0.50$ are shown along with scaled up versions of the weakest distortion. The scaling is done on the basis of the ratio of $p_{t,max}/p_{t,min} - 1$:

$$p_t \text{ factor} = \frac{(p_{t,max}/p_{t,min} - 1)_{\text{predicted}}}{(p_{t,max}/p_{t,min} - 1)_{\text{input}}}. \tag{9}$$

The (intensity $-$ 1) is used since otherwise the changes in total pressure variation between intensities would be under-represented. Using this scaling parameter, the shape of the circumferential variations in incidence are shown to be qualitatively similar and the circumferential locations of the maximum and minimum flow angle deviation from average occur at approximately the same location regardless of distortion intensity. To quantitatively interpret the incidence variation scaling relationships a normalized root mean squared (RMS) error is defined in a manner similar to in [2],

$$\hat{e}_{RMS} = \frac{e_{RMS}}{(\Delta\beta(\theta)_{\max} - \Delta\beta(\theta)_{\min})_{\text{actual}}}, \tag{10}$$

where

$$e_{RMS} = \sqrt{\frac{1}{2\pi}\int_{\theta=0}^{\theta=2\pi} \left((\Delta\beta)_{\text{predicted}} - (\Delta\beta)_{\text{actual}}\right)^2 d\theta}, \tag{11}$$

with equivalent definitions based on $\Delta\alpha$ for the stator. In the rotor, scaling up the weakest distortion response to the middle distortion (p_t factor $= 1.86$) yields a normalized RMS error between 1.77% and 3.67% in the rotor and between 1.06% and 2.16% in the stator. When scaling up to predict the most severe distortion intensity (p_t factor $= 2.44$), the discrepancy increases. Normalized RMS errors of 4.94% to 7.63% in the rotor and 3.20% to 6.03% in the stator are obtained. The p_t factor scaling consistently under-predicts the actual distortion effect on flow angle variation, though the absolute incidence prediction error is always less than 0.45°. The largest relative error resides in the inner span, which is likely due to upstream flow redistribution tending to alter the distortion profile shape over the hub.

That the linear scaling accuracy decreases as the distortion intensity is further increased suggests that an alternative approach may be better. $\Delta\beta$ and $\Delta\alpha$ cross zero at each span at the same circumferential locations for each of the distortion

intensities, which suggests that there may exist a (linear or non-linear) scaling parameter which would predict the behaviour even more accurately. In Fig. 13, the minimum intensity distortion is scaled up to the maximum intensity distortion such that the maxima at each span is matched. This scaling parameter is defined as

$$\kappa = \frac{(\Delta\beta_{max} - \Delta\beta_{min})_i}{(\Delta\beta_{max} - \Delta\beta_{min})_j}, \tag{12}$$

where i and j represent the two different distortion intensities the parameter is calculated between. This method guarantees that the maximum deviations in flow angle are matched, and provides an excellent estimate at capturing a more severe distortion's impact overall. The maximum excursions in flow angle and the circumferential extent of regions of positive incidence near the casing in the rotor are parameters which would be expected to relate to changes in overall blade row efficiency, as well as to govern stall margin reductions. To this point, Perovic et al. [17] were able to show that full rotating stall is generally limited to regions of high rotor incidence which are large enough to enable the stall cell to propagate around the entire annulus; regions of low or negative incidence tend to decay disturbances. Using this method, the maximum error again is found in the rotor at 25% span, but the value of normalized RMS error is reduced from 7.63% to 2.92%. While this scaling works well, it is a posteriori analysis that is not intended to generate a universal scaling value. It can be seen that there is no singular value that can appropriately scale up the effect on inlet flow angles, that is, κ is shown to vary somewhat with span for both blade rows. Instead, for BLI distortions of varying intensity, the relationship between total pressure distortion and inlet relative flow angle is more-than-linear and span dependent. This is illustrated in Fig. 14, in which values for the maximum extent of flow angle deviation is plotted against distortion intensity (minus one). The quotient of two points along an individual span line is κ. For each span plotted, both in the rotor and stator, a near linear relationship is observed for the lower distortion intensities. At the most severe intensity, the more than linear trend is revealed. The authors attempted various ways of defining the intensity scaling (e.g. ratio of maximum to minimum relative velocities squared) to attempt to collapse the curves at different span fractions, without success. Returning to the results shown, to quantify the degree of linearity, R^2 values for a linear regression passing through the origin are shown in Tab. 5 for both the rotor and the stator. The R^2 values obtained, greater than 0.972 for all spans in both blade rows, suggest that for the intensity variations considered in this paper, a posteriori maximum excursion scaling is an excellent method for predicting resultant inlet flow angle scaling. Inferences regarding distortion impact at intensities within this range presented can be made with confidence. The magnitude of values for $\Delta\alpha_{max} - \Delta\alpha_{min}$ in the stator is larger than that for $\Delta\beta_{max} - \Delta\beta_{min}$ in the rotor. This is expected as the rotor $\Delta\beta$ quantity is calculated in a frame of motion moving with a rotating blade and the frame transformation tends to reduce incidence variation. When the rotor quantities in Fig. 14 are calculated in the stationary frame, the magnitudes are similar to the stator and the separate curves move closer to one another. However, in designing a rotor blade, it is the relative frame flow angles that set the blade loading, therefore the relative frame quantity is reported here.

5.2 Vertically Stratified Distortion: Immersion Variation

Initially, flow angle deviation from the mean due to total pressure distortions increase as the immersion, $\delta/2R_0$, gets larger for both the rotor and stator. However the increase begins to saturate as $\delta/2R_0$ increases beyond 0.75, as shown in Fig. 15. This effect is most apparent at 75% span where the radial flow migration is minimal due to the proximity of the casing. Thus there is no clear scaling between the flow angle response of distortions of different immersions. In Fig. 16, values of maximum flow angle variations are plotted against distortion immersion. This plot reinforces the observation that upstream flow redistribution is highly non-linear with varying values of distortion immersion, especially in the rotor. In the rotor, the values for 25% span and 50% span cross over one another as the distortion extends to cover half of the hub. Beyond this value of immersion, each trend line has a similar less-than-linear behaviour. In the stator, this cross-over is not observed. This demonstrates that the magnitude of $\Delta\alpha_{max} - \Delta\alpha_{min}$ is dominated by the rotor outflow angle profile moreso than the far upstream distortion pattern.

5.3 Radially Stratified Distortion: Axis Offset From Compressor Axis

Consistent with low-speed results for diffusion factor variation in Defoe et al. [2], the distortion axis offset exhibits a non-linear flow angle variation behavior, shown in Fig. 17. Within the limits of $\Delta R/R_0 \leq 1.00$ changes to the distortion axis cause significant alterations to the compressor duct inlet distortion profile. For this reason, no linear scaling is expected. Beyond $\Delta R/R_0 = 1.00$, the distortion is not strongly altered and flow angle changes saturate. This is reinforced in Fig. 17 as the plots for $\Delta R/R_0 = 1.00$ and $\Delta R/R_0 = 1.50$ are nearly identical. The qualitative shape of the individual curves within the limit of $\Delta R/R_0 = 1.00$ do exhibit geometric similarities between axis offset variations. This is in direct contrast to the observations in Sec. 5.2, despite both studies observing the effect of changing the shape of the far upstream distortion. This is a due to the radial distortions inherently having a degree of similarity to the shape of the duct inlet itself, whereas the vertically stratified distortion has no geometric similarity to the duct at all. A plot of maximum variation in inlet flow angle versus distortion axis offset is presented in Fig. 18. The non-linearity of the distortion is clear in the rotor. The rotor trend lines are nearly linear until the distortion axis offset is aligned with the span fraction for each curve, this is clearly a result of the distortion shape. Sharp gradients in total enthalpy and total pressure are present near the distortion center which lead to stronger flow redistribution. When the distortion center is further away from the span line of interest, these sharper gradients are not present, and a near-linear behaviour is found. Due to distortion transfer through the rotor, the same behaviour is less apparent in the stator, though still present.

5.4 Radially Stratified Distortion: Intensity

The distortions of total enthalpy alone exhibit circumferential variations in flow angle of an order of magnitude less than those associated with total pressure distortions. This effect was observed by Defoe et al. [2] and is also found to be true for the distortions considered in this paper. In this section, distortions of both parameters combined are investigated, with the results also being virtually identical for total pressure alone distortions. Observations for radial distortions of varying intensity are consistent with those for the vertically stratified distortions; scaling of a weaker distortion based on total pressure

distortion intensity slightly under-predicts the effect on inlet relative flow angle. In Fig. 19, blade inlet flow angle variations are shown for a distortion axis offset of $\Delta R/2R_0 = 0.75$ for three different distortion intensities, $(dh_t/dr')(R_0/U^2_{mid}) = 0.0163, 0.0326,$ and 0.0489. The weakest distortion is again scaled up linearly using the factor κ. In both the rotor and stator, the predicted flow angle variation distributions are, as for the vertically stratified distortions, well captured. For the strongest distortion, the rotor flow angle variation error is nearly consistent at all spans; $\hat{e}_{RMS}$ ranges between 0.66% to 2.48% in the rotor and 0.70% to 3.03% in the stator. To confirm that this behavior does not deviate from that for vertically stratified distortions, maximum variations in flow angle are plotted against total pressure distortion intensity in Fig. 20 and the statistics of a linear regression through the origin are presented in Tab. 6. The behavior is closer to linear ($R^2 > 0.996$ for all spans in both blade rows) even though the distortion intensity magnitudes are similar to that for the vertically stratified distortion. The reason for this is due to the shape of the distortion itself. For a vertically stratified distortion with 50% immersion, the circumferential gradient from maximum to minimum total pressure is across one inlet duct radius. However, for the radial distortion (with $\Delta R/R_0 = 0.75$) a similar difference in minimum to maximum total pressure is spread across 1.75 inlet duct radii. This suggests it is the pitchwise gradients of total pressure which govern flow angle variation non-linearity. Therefore it is expected that further increases to distortion severity would reveal a similar slope to that seen for the vertically stratified case. In the stator, further flow redistribution through the rotor has occurred, moving each of the individual span lines closer to one another. It can therefore be stated for radially stratified distortions of varying intensity (even moreso than vertically stratified distortions) that a posteriori scaling based on maximum incidence excursion is valid. Within a practical distortion intensity range, incidence variations can be linearly scaled for different distortion intensities. Practical distortions are those which do not result in flow reversal at the computational domain inlet. Thus a useful approach is to compute the response for a strong distortion and scale down the response for weaker distortions that may be of interest.

6 Summary and Conclusions

In this paper, a body force model was used to numerically investigate blade row inlet flow angle variation with a variety of non-uniform inflow distortions for a transonic compressor. The distortions of interest are vertically stratified (boundary layer ingestion) and radially stratified (propeller axis offset from compressor axis) with varying far upstream intensity and geometric properties. Prior to this analysis, an investigation into the relationship between loss parameter and diffusion factor in a transonic machine was conducted to ensure that an appropriate scaling metric was employed.

The key outcomes of this work are that (1) diffusion factor was found to be an inaccurate method for quantifying streamwise loss generation for non uniform inflow as its empirical one-to-one relationship with loss parameter is valid only on-design. Instead, variations in blade inlet flow angles ($\Delta\beta$ and $\Delta\alpha$) were used to assess distortion impact since the body force model used does an excellent job of capturing these quantities, (2) highly non-linear inlet flow angle variation scaling was observed for varying far upstream distortion shape, especially for vertically stratified distortions, and (3) the inlet flow angle variations scale linearly with distortion intensity, especially when using a posteriori method of scaling the maximum flow angle excursions. The scaling is nearly perfectly linear as shown by the high R^2 values, but the slope changes with span, blade row, and distortion type. This type of scaling successfully predicts variations in flow angle all around the machine

circumference. The results suggest that it is the pitchwise gradients of the far upstream total pressure field which govern the linearity of the incidence variation scaling; larger gradients decrease the linearity of the response. This is consistent with the findings for diffusion factor for a low-speed fan in Defoe et al. [2]. Further work is required to quantify the exact levels of circumferential total pressure gradient that causes scaling to become non-linear.

The specific flow angle variation versus distortion intensity results obtained in this paper are expected only to hold for the machine studied (NASA stage 67) at the operating point selected. However, there is no reason to suggest that the observations made would not hold true for other low-speed or transonic axial fans and compressors as near-linear posteriori scaling was observed for two distinct distortion shapes. Additionally, the strongest distortions employed in this work represent the strongest practical distortion a commercial airliner could expect to experience in operation. Distortion intensities beyond the limit of this work would require regions of flow reversal, a phenomenon not expected with boundary layer ingestion or engine-runway interaction.

The significance of the findings are that they provide a way to expeditiously quantify the impact of various distortion intensities. A practical approach is to impose the strongest operating inlet distortion expected in a simulation, using either body force methods or higher-fidelity computations if deemed necessary. The results for incidence variation can then be scaled down linearly for lower distortion intensities without the need to run additional computations. Alternatively, from a single computation using some distortion intensity, the maximum distortion intensity which can be allowed given some limitation on acceptable incidence variations can be found using the linear scaling. Not only are the maximum flow angle variations well-captured with this approach, but the circumferential distributions of incidence are also well-predicted. This means that potential stall inception and fatigue loading for rotor blades can be assessed.

Future work should make use of a viscous loss model that is able to accurately capture local deviations from the peak efficiency flow coefficient such that scaling observations can be made directly from the local entropy generation along a streamline from a body force model.

Acknowledgements

This work is funded by the NSERC Discovery Grants program. It is based upon the work completed in Hill's thesis [18]. Computational resources are provided by the facilities of the Shared Hierarchical Academic Research Computing Network (SHARCNET:www.sharcnet.ca) and Compute/Calcul Canada. The authors would like to thank Dr. Ewan Gunn for the stage 67 stator model used in this work.

Nomenclature

A area

AR aspect ratio

b staggered blade spacing

B number of blades

$\overline{c}_{\text{in}-\text{out}}$ blade axial chord for a streamline

c_x blade axial chord

D diffusion factor

f force per unit volume

g_{red} rotor reduced frequency

h enthalpy

K_{p1}, K_{p2} body force viscous loss model coefficients

$\dot{m}$ corrected mass flow rate

M Mach number

p pressure

r radial coordinate

r' radial coordinate from propeller axis

R radius

ΔR propeller axis offset from compressor axis

s entropy

T temperature

U_{mid} midspan blade speed

V velocity in stationary frame

W velocity in relative frame

x, y, z Cartesian coordinates

Z loss parameter

α absolute flow angle

β relative flow angle

γ ratio of specific heats

δ distortion immersion

ζ loss coefficient

η efficiency

θ circumferential coordinate

θ^* boundary layer momentum thickness

π total pressure ratio

ρ density

σ blade solidity

ϕ flow coefficient

ω corrected rotational speed

Subscripts

$0-3$ axial measurement planes

is isentropic

n component normal to relative streamline

p component parallel to relative streamline

ref reference value

rel relative frame quantity

RMS root mean square

t total/stagnation quantity

Superscripts

M mass-averaged quantity

θ circumferentially-averaged quantity

References

[1] Gunn, E., and Hall, C., 2014. "Aerodynamics of boundary layer ingesting fans". In ASME Turbo Expo 2014: Turbine Technical Conference and Exposition, American Society of Mechanical Engineers. Paper V01AT01A024.

[2] Defoe, J., Etemadi, M., and Hall, D., 2018. "Fan performance scaling with inlet distortions". *ASME J. Turbomach.,* **140**(7), p. 071009.

[3] Fidalgo, V., Hall, C., and Colin, Y., 2012. "A study of fan-distortion interaction within the nasa rotor 67 transonic stage". *ASME J. Turbomach.,* **134**(5). Paper 051011.

[4] Hall, D., Greitzer, E., and Tan, C., 2017. "Analysis of fan stage conceptual design attributes for boundary layer ingestion". *ASME J. Turbomach.,* **139**(7). Paper 071012.

[5] Gunn, E. J., and Hall, C. A., 2019. "Nonaxisymmetric stator design for boundary layer ingesting fans". *ASME J. Turbomach.,* **141**(7), p. 071010.

[6] Hill, D. J., and Defoe, J. J., 2018. "Innovations in body force modeling of transonic compressor blade rows". *International Journal of Rotating Machinery,* **2018**.

[7] Peters, A., Spakovszky, Z., Lord, W., and Rose, B., 2015. "Ultrashort nacelles for low fan pressure ratio propulsors". *ASME J. Turbomach.,* **137**(2). Paper 021001.

[8] Kerrebrock, J. L., 1992. *Aircraft engines and gas turbines*. MIT press Cambridge, MA.

[9] Strazisar, A., Wood, J., Hathaway, M., and Suder, K., 1989. Laser anemometer measurements in a transonic axial-flow fan rotor, Nov.

[10] Lieblein, S., Schwenk, F. C., and Broderick, R. L., 1953. Diffusion factor for estimating losses and limiting blade loadings in axial-flow-compressor blade elements. Tech. rep., National Advisory Committe for Aeronautics, Lewis Flight Propulsion Lab.

[11] Lieblein, S., 1965. "Experimental flow in two-dimensional cascades". *NASA Special Publication,* **36**, p. 183.

[12] ANSYS, INC., 2013. *ANSYS CFX Solver Theory Guide*, release 15.0 ed. Canonsburg, PA, November.

[13] POINTWISE, 2016. *Pointwise User's Manual*, 18.0r2 ed. Forth Worth, TX.

[14] ANSYS, INC., 2013. *ANSYS TurboGrid User's Guide*, release 15.0 ed. Canonsburg, PA, November.

[15] Menter, F., 1993. "Zonal two-equation k-ω turbulence model for aerodynamic flows". *AIAA Paper*(1993-2906).

[16] Gunn, E. J., Tooze, S. E., Hall, C. A., and Colin, Y., 2013. "An experimental study of loss sources in a fan operating with continuous inlet stagnation pressure distortion". *ASME J. Turbomach.,* **135**(5), p. 051002.

[17] Perovic, D., Hall, C. A., and Gunn, E., 2019. "Stall inception in a boundary layer ingesting fan". *ASME J. Turbomach.,* **141**(9), p. 091007.

[18] Hill, D., 2017. "Compressor performance scaling in the presence of non-uniform flow". Master's thesis, University of Windsor (Canada).

Table 1. Experimental performance characteristics for NASA stage 67 rotor at peak-efficiency and 90% corrected rotational speed [3].

Parameter	Rotor
corrected angular speed Ω (rad/s)	1.51×10^3
$M_{\text{rel,tip}}$	1.20
total-to-total pressure ratio $\overline{p}_{t2}^{M}/\overline{p}_{t1}^{M}$	1.48
corrected mass flow rate $\dot{m}$ (kg/s)	31.1
peak isentropic efficiency η_{is} (%)	92.2
peak efficiency flow coefficient, ϕ	0.498

Table 2. Geometric characteristics for NASA stage 67 rotor and stator [3].

Parameter	Rotor	Stator
hub solidity σ_{hub}	3.11	2.57
tip solidity σ_{tip}	1.29	1.33
$\frac{r_{\text{hub}}}{r_{\text{tip}}}$ inlet	0.375	0.50
$\frac{r_{\text{hub}}}{r_{\text{tip}}}$ outlet	0.478	0.53
$\frac{\text{tip clearance}}{r_{\text{tip}}}$	0.0039	-
number of blades B	22	36
aspect ratio AR	1.56	2.16

Table 3. Single-passage RANS grid convergence parameters at peak efficiency and 90% corrected rotational speed.

	Medium Grid	Fine Grid	% Change
rotor cell count	1.78×10^6	2.45×10^6	37.6
$\pi_{rotor} - 1$	0.493	0.496	0.71
rotor η_{is}	92.3%	92.3%	0

Table 4. Distortions considered.

	Vertically stratified		Radially stratified		
	$\frac{p_{t,\max}}{p_{t,\min}}$	$\left(\frac{\delta}{2R_0}\right)$	$\left(\frac{dp_t}{dr}\right)\left(\frac{R_0}{\bar{\rho}_1^M U_{\text{mid}}^2}\right)$	$\left(\frac{dh_t}{dr}\right)\left(\frac{R_0}{U_{\text{mid}}^2}\right)$	$\left(\frac{\Delta R}{R_0}\right)$
Total pressure	1.050	0.50			
	1.093	0.25			
	1.093	0.50			
	1.093	0.75			
	1.093	1.00			
	1.122	0.50			
Total pressure			0.0184		0.75
			0.0371		0.25
			0.0371		0.50
			0.0371		0.75
			0.0572		0.75
Total temperature				0.0163	0.75
				0.0326	0.25
				0.0326	0.50
				0.0326	0.75
				0.0489	0.75
Combined			0.0185	0.0163	0.75
			0.0381	0.0326	0.00
			0.0380	0.0326	0.25
			0.0379	0.0326	0.50
			0.0377	0.0326	0.75
			0.0374	0.0326	1.00
			0.0585	0.0489	0.75

Table 5. Linear regression statistics for vertically stratified distortions of total pressure with $\delta/2R_0 = 0.50$.

	Rotor		**Stator**	
Span %	Slope	R^2	Slope	R^2
25	11.8	0.972	45.1	0.983
50	25.3	0.987	53.4	0.991
75	46.3	0.990	70.5	0.996

Table 6. Linear regression statistics for radially stratified distortions with $\Delta R/R_0 = 0.75$.

	Rotor		**Stator**	
Span %	Slope	R^2	Slope	R^2
25	24.5	0.998	62.6	0.996
50	43.4	0.999	70.4	0.999
75	53.9	0.997	72.8	1.000

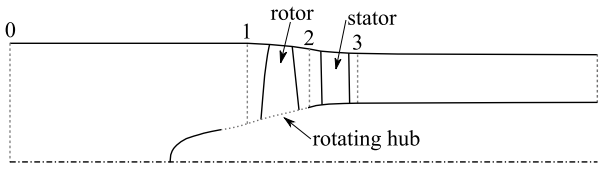

Fig. 1. Meridional view of the computational domain with axial measurement stations.

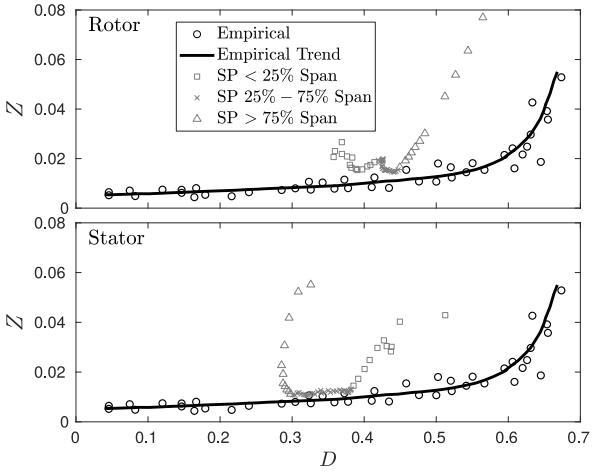

Fig. 2. Loss parameter versus diffusion factor for single passage RANS for stage 67 at 90% corrected rotational speed for uniform inflow, $\phi = 0.498$. Empirical data adapted from Kerrebrock [8].

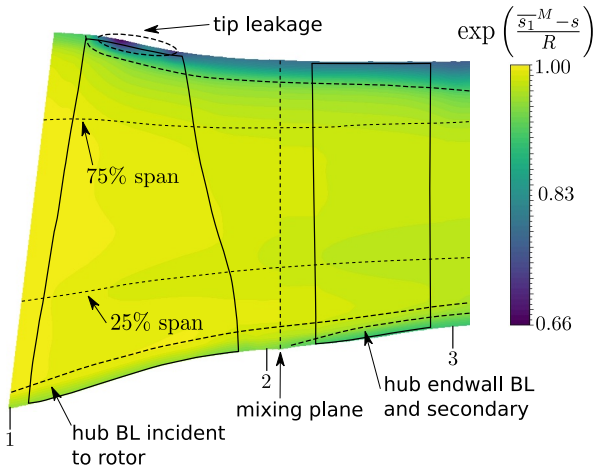

Fig. 3. Contours of circumferentially averaged entropy function for single passage RANS for stage 67 at 90% corrected rotational speed for uniform inflow at design flow coefficient, $\phi = 0.498$.

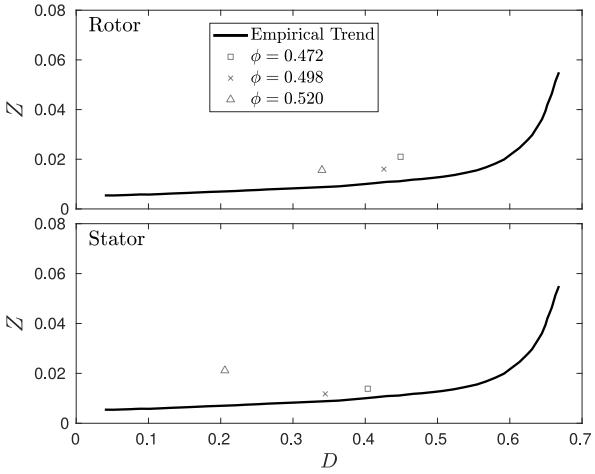

Fig. 4. Relationship between loss parameter and diffusion at flow coefficients both on and off design flow coefficient for single passage RANS for stage 67 at 90% corrected rotational speed with uniform inflow, compared against experimental data from Kerrebrock [8].

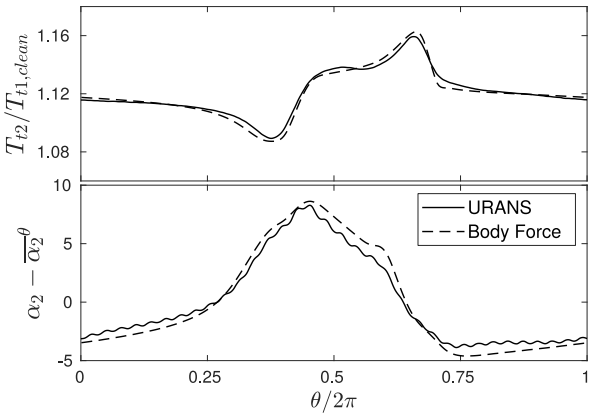

Fig. 5. Circumferential traverse of rotor trailing edge swirl angle and total temperature at midspan. Body force results [6] and Fidalgo et al. URANS [3].

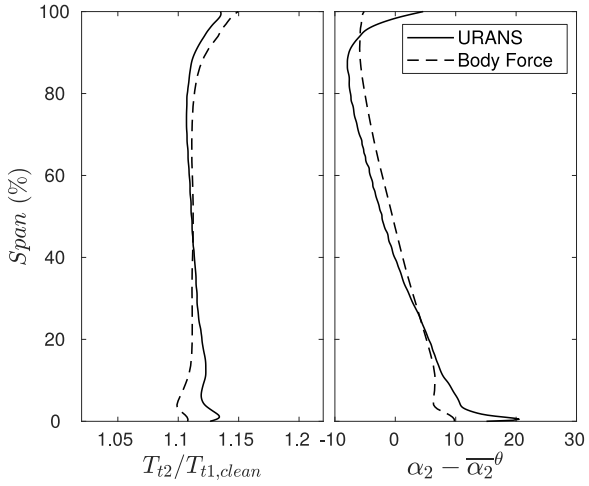

Fig. 6. Radial traverse of rotor trailing edge swirl angle and total temperature at circumferential coordinate corresponding to the center of distortion upstream of the rotor. Body force results [6] and Fidalgo et al. URANS [3].

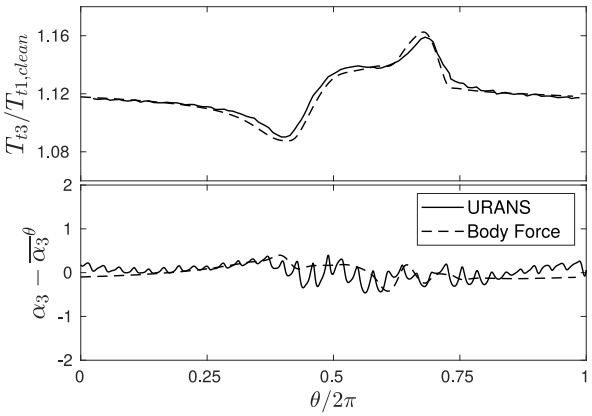

Fig. 7. Circumferential traverse of stator trailing edge swirl angle and total temperature at midspan. Body force results [6] and Fidalgo et al. URANS [3].

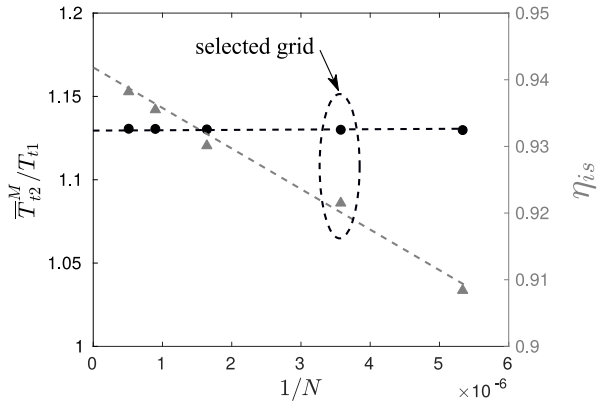

Fig. 8. Rotor work input (circles, left axis) and rotor isentropic efficiency (crosses, right axis) at peak efficiency for stage 67 at 90% corrected rotational speed for various body force grid cell counts.

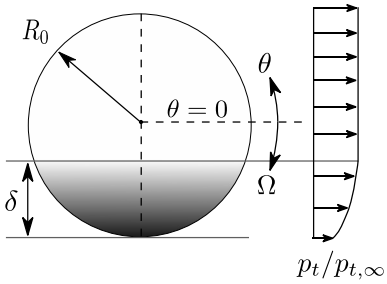

Fig. 9. Vertically stratified inlet distortion schematic, adapted from [2].

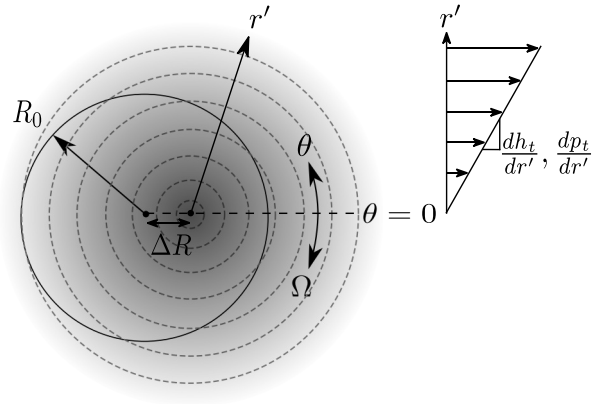

Fig. 10. Radially stratified distortion schematic, showing propeller work input contour lines offset from the compressor duct inlet, adapted from [2].

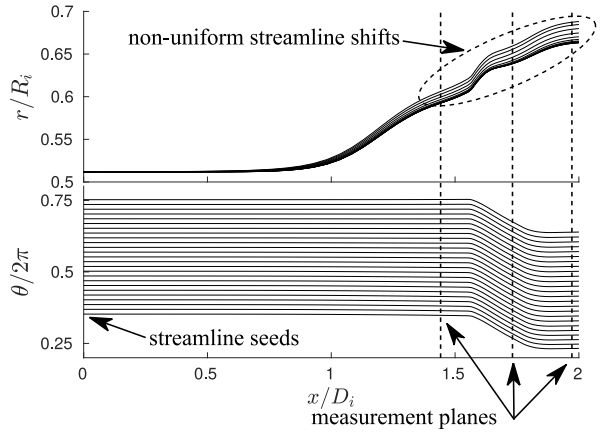

Fig. 11. Illustration of streamline tracking used to extract data from non-uniform inflow body force computations. Example shown is half-annulus of vertically stratified distortion at 50% inlet span with $\delta/2R_0 = 0.50$ and $p_{t,\max}/p_{t,\min} = 1.122$.

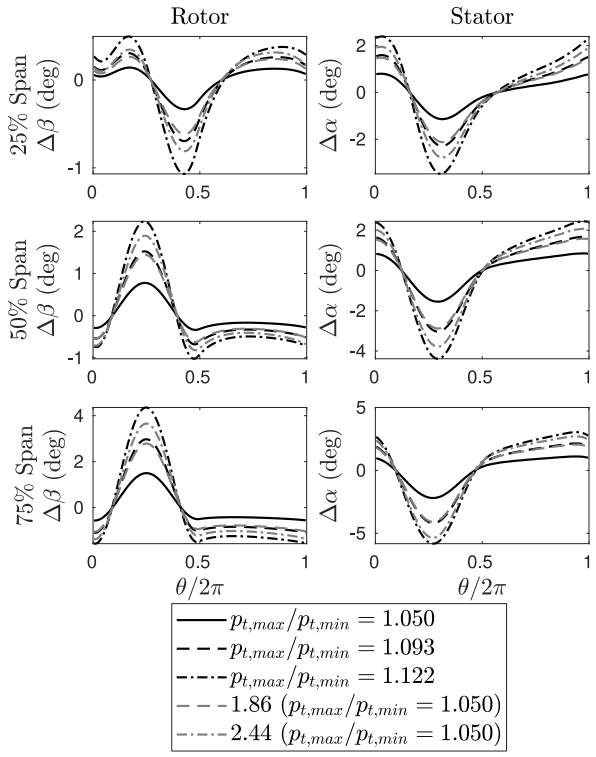

Fig. 12. Circumferential traverses of flow angle changes at 25%, 50%, and 75% span for vertically stratified distortions of varying $p_{t,\max}/p_{t,\min}$ with $\delta/2R_0 = 0.50$ and scaled based on p_t factor to the medium (m) and strong (s) distortion.

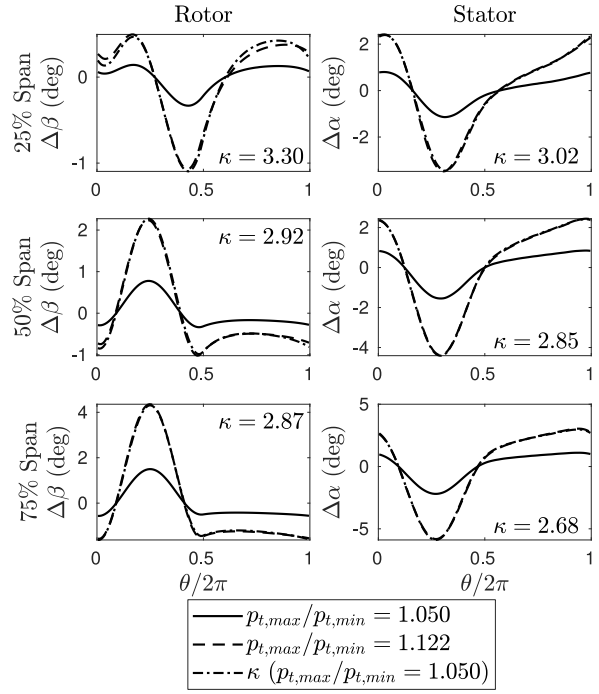

Fig. 13. Circumferential traverses of flow angle changes at 25%, 50%, and 75% span for rectilinear distortions of varying $p_{t,\max}/p_{t,\min}$ with $\delta/2R_0 = 0.50$ and scaled based on κ.

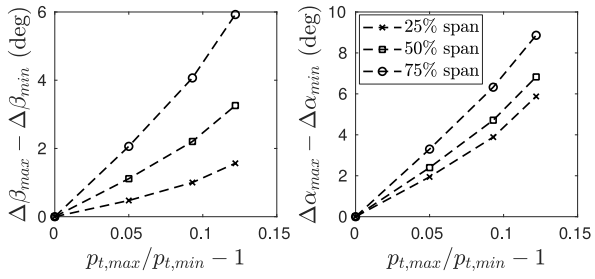

Fig. 14. Maximum variation in inlet flow angle versus distortion total pressure intensity for the rotor (left) and stator (right) for vertically stratified distortions of total pressure with $\delta/2R_0 = 0.50$.

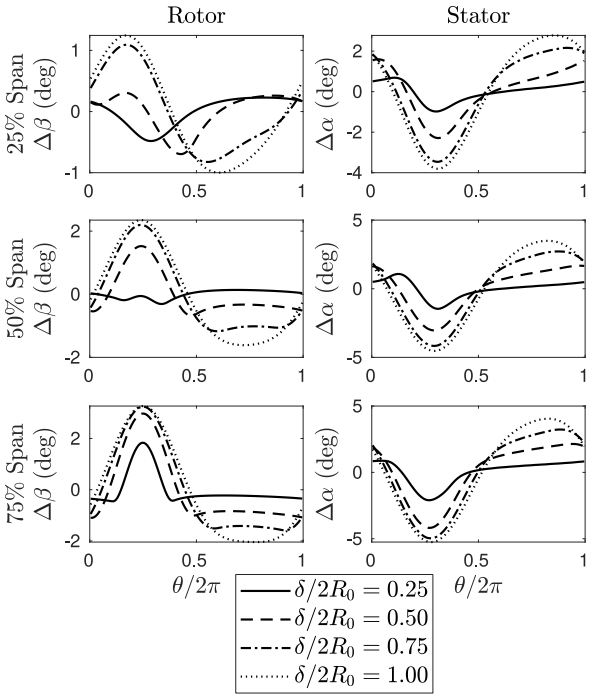

Fig. 15. Circumferential traverses of loss parameter changes at 25%, 50%, and 75% span for rectilinear distortions of varying $\delta/2R_0$ with $p_{t,\max}/p_{t,\min} = 1.093$.

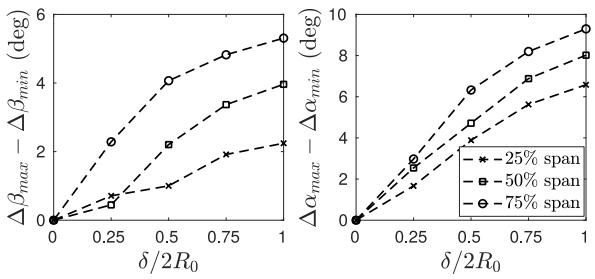

Fig. 16. Maximum variation in inlet flow angle versus distortion immersion for the rotor (left) and stator (right) for vertically stratified distortions of total pressure with $p_{t,\max}/p_{t,\min} = 1.093$.

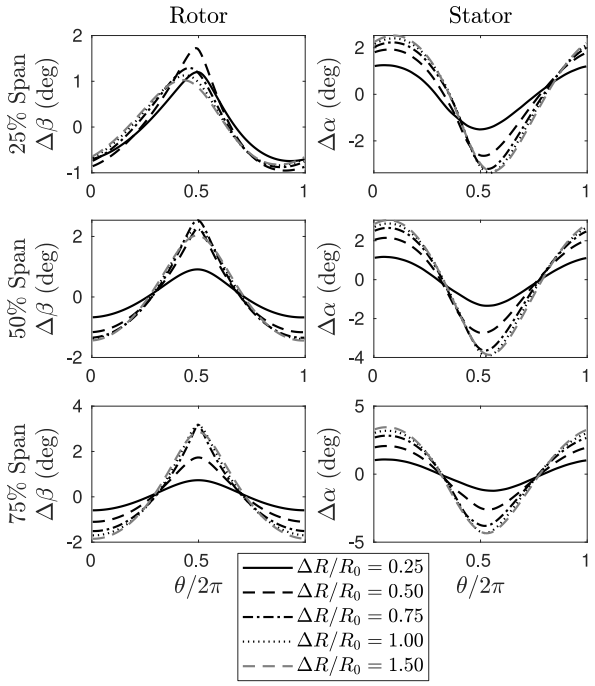

Fig. 17. Circumferential traverses of flow angle changes at 25%, 50%, and 75% span for radially stratified distortions with $(dh_t/dr')(R_0/U_{mid}^2) = 0.0326$ and $(dp_t/dr')(R_0/\bar{\rho}_1^M U_{mid}^2) = 0.038$.

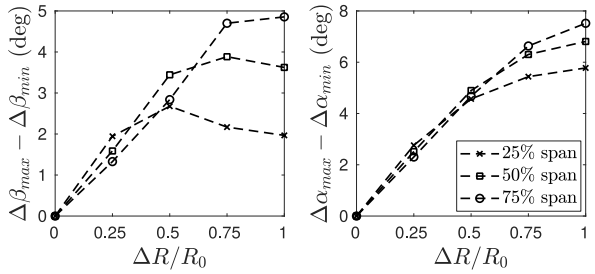

Fig. 18. Maximum variation in inlet flow angle versus distortion axis offset for the rotor (left) and stator (right) for radially stratified distortions with $(dh_t/dr')(R_0/U_{mid}^2) = 0.0326$ and $(dp_t/dr')(R_0/\bar{\rho}_1^M U_{mid}^2) = 0.038$.

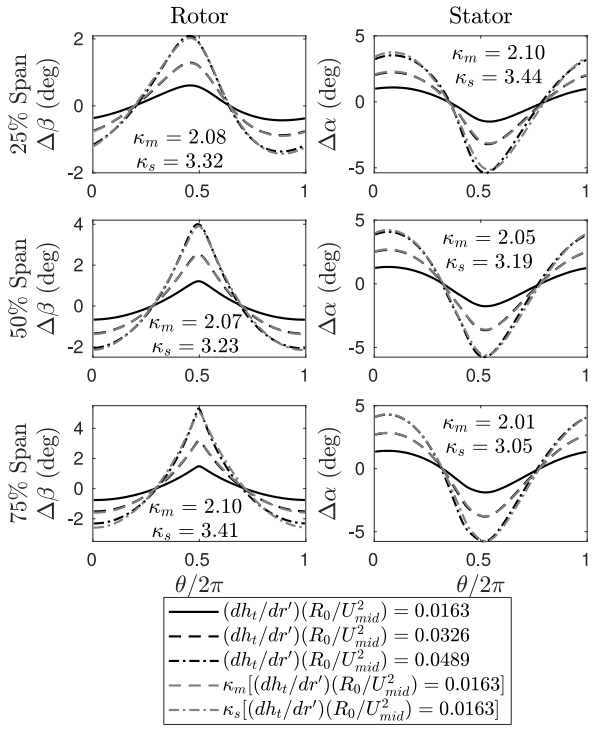

Fig. 19. Circumferential traverses of flow angle changes at 25%, 50%, and 75% span for radially stratified distortions with $\Delta R/R_0 = 0.75$ and scaling up to the medium (m) and strong (s) distortion.

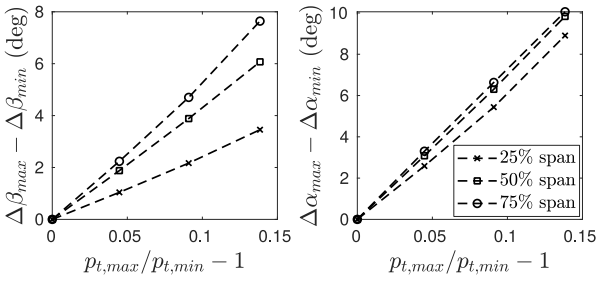

Fig. 20. Maximum variation in inlet flow angle versus distortion total pressure intensity for the rotor (left) and stator (right) for radially stratified distortions with $\Delta R/R_0 = 0.75$.